



## Research Article

# Fractional Modeling of Non-Newtonian Casson Fluid between Two Parallel Plates

Mubashir Qayyum , Sidra Afzal , and Efaza Ahmad

*Department of Sciences and Humanities, National University of Computer and Emerging Sciences-FAST Lahore Campus, Lahore, Pakistan*

Correspondence should be addressed to Mubashir Qayyum; [mubashir.qayyum@nu.edu.pk](mailto:mubashir.qayyum@nu.edu.pk)

Received 26 November 2022; Revised 10 February 2023; Accepted 21 February 2023; Published 8 March 2023

Academic Editor: Serkan Araci

Copyright © 2023 Mubashir Qayyum et al. This is an open access article distributed under the Creative Commons Attribution License, which permits unrestricted use, distribution, and reproduction in any medium, provided the original work is properly cited.

In this manuscript, fractional modeling of non-Newtonian Casson fluid squeezed between two parallel plates is performed under the influence of magneto-hydro-dynamic and Darcian effects. The Casson fluid model is fractionally transformed through mixed similarity transformations. As a result, partial differential equations (PDEs) are transformed to a fractional ordinary differential equation (FODE). In the current modeling, the continuity equation is satisfied while the momentum equation of the integral order Casson fluid is recovered when the fractional parameter is taken as  $\alpha = 1$ . A modified homotopy perturbation algorithm is used for the solution and analysis of highly nonlinear and fully fractional ordinary differential equations. Obtained solutions and errors are compared with existing integral order results from the literature. Graphical analysis is also performed at normal and radial velocity components for different fluid and fractional parameters. Analysis reveals that a few parameters are showing different behavior in a fractional environment as compared to existing integer-order cases from the literature. These findings affirm the importance of fractional calculus in terms of more generalized analysis of physical phenomena.

## 1. Introduction

Scientists and researchers around the globe are recently more focused on capturing fractional phenomena instead of integer-order problems. A major reason for considering fractional environment is to consider a more general problem with memory effect that is helpful in many engineering and physical issues. In this regard, different types of fractional derivatives are considered in which various kernels are involved. Chu et al. [1] analyzed MHD flow of a Newtonian fluid containing hybrid nanoparticles through an ABC fractional model by utilizing the Laplace transform method. They studied temperature and velocity profiles for water, kerosene, and engine oil. Kang et al. investigated [2] a time-variant traffic flow model in fractional order by using the modeling principle of the Bass model. The results of this fractional model were compared with six other traffic models to check efficiency. Yavuz et al. [3] studied fractional second-

grade fluid model by using the classical Caputo fractional operator. Exact solutions to the problem were computed through the Laplace transform method. Ferromagnetic fluid was analyzed by Abro [4] through the fractal-Laplace transform. A fractal-fractional differential operator was used in modeling that was principally focused on power law. Chen et al. [5] analyzed service of data latency through the fractional fluid model use network systems with multi-hop. Rate-type fluid models are presented by Abro and Atangana [6] using nonlocal differentiation. Reyaz et al. [7] studied fractional Casson fluid flow under impact of thermal radiation passing over an oscillating plate. Arif et al. [8] investigated engine oil characteristics at ramped wall temperature using a fractional Casson fluid model. Prabhakar's fractional approach on Casson fluid with generalized Fourier law was studied by Sarwar et al. [9]. Ur Rehman et al. [10] fractionally analyzed Casson fluid with Fourier and Fick's laws. Electro-osmotic flow of a fractal-fractional

modeled Casson fluid was examined by Murtaza et al. [11] by using a finite difference approach for solution purposes.

Non-Newtonian fluids have many applications in chemical engineering, mechanical, industrial, and biological fields due to their visco-elastic properties. Non-Newtonian fluids do not obey Newton's law of viscosity and behave differently under varying physical conditions. Many researchers have analyzed different non-Newtonian fluid models in the literature. Gireesha et al. [12] studied the two-phase flow of a Maxwell fluid with a heat source and sink. Mahanthesh et al. [13] then analyzed the three-dimensional flow of Maxwell fluid flow impacted by the nonlinear thermal radiation effect. Krupalakshmi et al. [14] simulated two-dimensional steady flow of a non-Newtonian fluid over a heated stretching sheet. Das et al. [15] analyzed flow of an ethylene glycol-based hybrid nanofluid with special reference to entropy generation. The flow of a nanofluid influenced by quadratic radiative heat flux is simulated by Mahanthesh [16]. Casson fluids possess shear thinning properties and are hence much useful in manufacturing of paints, extraction of crude oil, and the food industry. Divya et al. [17] investigated peristaltic flow in the Casson fluid model influenced by a magnetic field in the radial direction passing through a nonuniform channel. Thermal properties were studied under convective boundary conditions. This model characterized blood flow through arterial walls. Khan and Ali [18] gave a theoretical analysis of the classical Graetz problem for the model of Casson fluid. A built-in technique called `bvp4c` was employed to solve the flow problem. El-Kabeir et al. [19] examined the mixed convective flow of a Casson nanofluid with partial slip at the boundary. Aneja et al. [20] studied the flow of Casson fluid through a partially heated porous square cavity with natural convection. The finite element method was utilized to solve the system of highly nonlinear coupled equations. Fluid flow and heat transfer of Casson fluid passing through a partially heated trapezoidal cavity were scrutinized by Hamid et al. [21]. For solution purpose, the finite element method was employed with the Galerkin optimizer. Rashidi et al. [22] analyzed blood flow through the Casson fluid model with special reference to heat and mass transfer. Das et al. [23, 24] analyzed Casson nanofluid with copper nanoparticles in a porous microchannel. Vs and Pai [25] studied Casson fluid flow between two plates with suction and injection phenomena. The flow problem is solved by using the homotopy perturbation technique and compared with a finite difference scheme. Hamarshah et al. [26] simulated the Casson nanofluid's natural convective flow over a horizontal cylinder with methanol-base fluid. Alwawi et al. [27] numerically analyzed the heat transfer effects of Casson nanofluid over a solid sphere. Several other Casson fluid models are scrutinized by researchers in literature [28–30].

In order to solve governing differential equations of flow problems various analytical and semi-numerical approaches are employed. Due to the highly nonlinear and fractional nature of the current problem, we apply a hybrid of the Laplace transform with the homotopy perturbation algorithm. Many fractional problems in various fields of mathematics and engineering have recently been solved

using this technique due to its efficiency in tackling fractional environment. Morales-Delgado et al. [31] used the Laplace homotopy perturbation technique to solve the coupled system of the time-fractional Keller–Segal chemotaxis model with nonsingular kernel. Qayyum et al. [32] studied soliton solutions of the Korteweg–de Vries system with the help of a Laplace transform and homotopy perturbation technique. Dispersive long-wave and Hirota–Satsuma KdV systems were solved, and better results were obtained through LHPM when compared with existing results in the literature. Coupled Whitham–Broer–Kaup equations in fractional order were investigated by Nonlaopon et al. [33] with Mittag–Leffler and exponential laws in Caputo sense of fractional derivatives. The system of partial differential equations was solved with the help of the Laplace transform coupled with the homotopy perturbation method. Sulaiman et al. [34] studied fractional viscous Burgers' equations with kernels of Mittag–Leffler type utilizing Laplace transform with homotopy perturbation technique. The uniqueness and existence of the proposed model were validated and the effect of various parameters on displacement was studied graphically. Ahmad et al. [35] solved a third order fractional PDE undergoing exponential decay by utilizing the LHPM scheme to tackle a fractional derivative with Mittag–Leffler type kernel. Shokhanda et al. [36] analyzed a two-mode fractional Burgers' equation with the LHPM technique. Yavuz and Ozdemir [37] used the inverse Laplace homotopy perturbation scheme to numerically investigate the fractional heat equations. Pandey et al. [38] computed approximate solutions for the space and time fractional diffusion equation in two dimensions using the Laplace transform with homotopy perturbation method. Fang et al. [39] used the same semi-analytical approach to find solutions for the fractionally ordered Camassa–Holm equation. Pandey et al. [40] applied the Laplace homotopy perturbation scheme to reaction diffusion equations in fractional order to evaluate the approximate series solution. Nonlinear time-fractional differential equations were evaluated by Zhang et al. [41] by employing the LHPM algorithm. This technique was also utilized by Jalili et al. [42] to work out the approximate results for a Newtonian fluid model at fractional order.

This study focuses on fractional modeling and simulation of an unsteady Casson fluid model squeezed between two plates under magneto-hydro-dynamic effect and porosity. A literature review reveals that the unsteady Casson fluid flow has not been modeled in a fractional environment and thoroughly analyzed along with error analysis and solution validation. In this regard, the unsteady Casson fluid model is fractionally transformed into a more general and comprehensive fluid model in fractional order. This complex model is solved by utilizing the modified homotopy perturbation technique. Residual errors are computed and compared with existing results in the literature. Graphical analysis is done to analyze the behavior of fluid flow with varying fluid parameters. This study is divided into the following sections. Section 1.1 provides basic definitions, Section 2 presents problem formulation and mathematical modeling, methodology used to solve the flow problem is

given in Section 3, results are discussed in Section 4 and finally, conclusions are made in Section 5.

1.1. Preliminaries

Definition 1. The Caputo fractional derivative  $\mathcal{D}^\alpha$  of a function  $\mathcal{Y}(\mathbf{u})$  can be expressed as follows [43]:

$$\mathcal{D}^\alpha\{\mathcal{Y}(\mathbf{u})\} = \frac{1}{\Gamma(r-\alpha)} \int_0^{\mathbf{u}} (\mathbf{u}-\tau)^{r-\alpha-1} \mathcal{Y}^{(r)}(\mathbf{u}) d\tau, \quad r-1 < \alpha \leq r. \tag{1}$$

Definition 2. The Laplace transform  $\mathfrak{L}$  of Caputo's fractional derivative  $\mathcal{D}^\alpha$  is as follows [44]:

$$\mathfrak{L}\{\mathcal{D}^\alpha \mathcal{Y}(\mathbf{u})\} = s^\alpha \mathfrak{L}\{\mathcal{Y}(\mathbf{u})\} - \sum_{n=0}^{k-1} s^{\alpha-n-1} \mathcal{Y}^{(n)}(0), \quad r-1 < \alpha \leq r. \tag{2}$$

2. Mathematical Formulation of Fractional Casson Fluid

A detailed modeling and mathematical formulation of non-Newtonian fractional Casson fluid is given in the following steps.

2.1. Fluid Model. Consider an incompressible flow of a Casson fluid passing between two plates that are  $h(t)$  distance apart in the  $z$ -direction. We define  $h(t) = \pm L(1 - \gamma t)^{1/2}$ , where  $\gamma$  represents squeezing motion of both plates and  $L$  is the initial gap among the plates. Squeezing motion of plates is characterized by  $\gamma > 0$  whereas plates recede when  $\gamma < 0$ . Major flow assumptions are as follows:

- (i) Fluid is at rest at time  $t = 0$  between two plates distance  $h(t)$  apart.

- (ii) Fluid motion is caused by squeezing/receding motion between two plates at  $t > 0$ .
- (iii) Magneto-hydro-dynamic effect acts perpendicular to the axis  $y = 0$  along with Darcian effects.
- (iv) The stress tensor of incompressible Casson fluid is given as follows [28–30].

$$\tau_{ij} = \begin{cases} 2 \left[ \mu_B + \frac{P_y}{2\pi_c} \right] e_{ij}, & \pi > \pi_c, \\ 2 \left[ \mu_B + \frac{P_y}{2\pi_c} \right] e_{ij}, & \pi_c > \pi. \end{cases} \tag{3}$$

The governing equations of flow characterized by the mentioned assumptions are as follows [45]:

$$\frac{\partial u}{\partial x} + \frac{\partial v}{\partial y} = 0, \tag{4}$$

$$\frac{\partial u}{\partial t} + u \frac{\partial u}{\partial x} + v \frac{\partial u}{\partial y} = -\frac{1}{\rho} \frac{\partial p}{\partial x} + \nu \left( 1 + \frac{1}{\beta} \right) \left( 2 \frac{\partial^2 u}{\partial x^2} + \frac{\partial^2 u}{\partial y^2} + 2 \frac{\partial^2 v}{\partial y \partial x} \right) - \frac{\sigma B^2}{\rho} u - \frac{\mu}{\rho k} u, \tag{5}$$

$$\frac{\partial v}{\partial t} + u \frac{\partial v}{\partial x} + v \frac{\partial v}{\partial y} = -\frac{1}{\rho} \frac{\partial p}{\partial y} + \nu \left( 1 + \frac{1}{\beta} \right) \left( 2 \frac{\partial^2 v}{\partial x^2} + \frac{\partial^2 v}{\partial y^2} + 2 \frac{\partial^2 u}{\partial y \partial x} \right) - \frac{\mu}{\rho k} v. \tag{6}$$

This flow problem is subject to the following boundary conditions:

$$\left. \begin{aligned} u &= 0 \\ v &= v_w = \frac{dh}{dt} \end{aligned} \right\} \text{ at } y = h(t),$$

$$\left. \begin{aligned} \frac{\partial v}{\partial y} &= 0 \\ v &= 0 \end{aligned} \right\} \text{ at } y = 0.$$
(7)

Now, we introduce a vorticity function  $\omega$  as follows:

$$\omega = \left( \frac{\partial v}{\partial x} - \frac{\partial u}{\partial y} \right). \quad (8)$$

Final velocity equation is obtained by using equations (5) and (6) in equation (8), which is given as follows:

$$\frac{\partial \omega}{\partial t} + u \frac{\partial \omega}{\partial x} + v \frac{\partial \omega}{\partial y} = \nu \left( 1 + \frac{1}{\beta} \right) \left( \frac{\partial^2 \omega}{\partial x^2} + \frac{\partial^2 \omega}{\partial y^2} \right) - \frac{\sigma B^2}{\rho} \frac{\partial u}{\partial y} - \frac{\mu}{\rho k} \omega. \quad (9)$$

**2.2. Similarity Transformations.** The similarity transforms for unsteady squeezing flow of fractional Casson fluid are as follows [45, 46]:

$$\eta = \frac{y}{L(1-\gamma t)^{1/2}},$$

$$u = \frac{\gamma x}{2(1-\gamma t)} U'(\eta),$$

$$v = \frac{-L\gamma}{2(1-\gamma t)^{1/2}} U(\eta),$$
(10)

and

$$\psi(x, y, t, \eta(y, t)) = \frac{\gamma L x U(\eta^\alpha)}{2\sqrt{1-\gamma t}},$$

$$\eta^\alpha(y, t) = \frac{y^\alpha}{L\Gamma(\alpha+1)\sqrt{1-\gamma t}},$$

$$\psi_y = u$$

$$= \frac{\alpha \gamma x y^{\alpha-1} U^\alpha(\eta^\alpha)}{2\Gamma(\alpha+1)(1-\gamma t)},$$

$$\psi_x = v = \frac{-\gamma L U(\eta^\alpha)}{2\sqrt{1-\gamma t}},$$
(11)

where  $\alpha$  is the fractional parameter such that  $0 < \alpha \leq 1$ .

### 2.3. Nondimensionalization in Fractional Environment

**2.3.1. Continuity Equation.** By introducing equation (11) in equation (4), we check that fractional transform satisfies the continuity equation identically.

**2.3.2. Momentum Equation.** The momentum equation in equation (9) is fractionally nondimensionalized by using equation (11) as follows:

$$\begin{aligned} & \kappa_t \left( (\alpha-1)\alpha\eta^{\alpha-2}(-U^\alpha) - \alpha^2\eta^{2\alpha-2}U^{2\alpha} \right) + M_t \left( \alpha^2\eta^{2\alpha-2}U^{2\alpha} + (\alpha-1)\alpha\eta^{\alpha-2}U^\alpha \right) \\ & + Sq \left( \begin{aligned} & \alpha^3 u \eta^{3\alpha-3} U^{3\alpha} - (\alpha-1)\alpha^2 \eta^{2\alpha-3} U^{3\alpha} - \alpha^2 (2\alpha-2) \eta^{2\alpha-3} U^{3\alpha} - 3\alpha^2 \eta^{2\alpha-2} U^{2\alpha} \\ & - \alpha^2 \eta^{3\alpha-2} U^{3\alpha} + (\alpha-2)(\alpha-1)\alpha\eta^{\alpha-3} U^{2\alpha} - (\alpha-1)\alpha\eta^{2\alpha-2} U^{2\alpha} \\ & - (\alpha-1)\alpha^2 \eta^{2\alpha-3} (U^\alpha)^2 - 2(\alpha-1)\alpha\eta^{\alpha-2} U^\alpha - \alpha^3 \eta^{3\alpha-3} U^{2\alpha} U' \end{aligned} \right) \\ & + \left( \frac{1}{\beta} + 1 \right) \left( \begin{aligned} & (\alpha-3)(\alpha-2)(\alpha-1)\alpha\eta^{\alpha-4} U^\alpha + (\alpha-2)(\alpha-1)\alpha^2 \eta^{2\alpha-4} U^{2\alpha} + (\alpha-1)\alpha^3 \eta^{3\alpha-4} U^{3\alpha} \\ & + \alpha^4 \eta^{4\alpha-4} U^{4\alpha} + \alpha^3 (2\alpha-2)\eta^{3\alpha-4} U^{3\alpha} + \alpha^3 (3\alpha-3)\eta^{3\alpha-4} U^{3\alpha} \\ & + \alpha^2 (2\alpha-3)(2\alpha-2)\eta^{2\alpha-4} U^{2\alpha} + (\alpha-1)\alpha^2 (2\alpha-3)\eta^{2\alpha-4} + U^{2\alpha} \end{aligned} \right) \\ & = 0, \end{aligned} \quad (12)$$

where the dimensionless quantities are defined as follows:

$$\begin{aligned}
 Sq &= \frac{\gamma L^2}{2\nu}, \\
 M &= \frac{L^2 \sigma B^2}{\rho \nu}, \\
 M_t &= M(1 - \gamma t), \\
 \kappa &= \frac{\nu}{k\gamma}, \\
 \kappa_t &= \kappa(1 - \gamma t),
 \end{aligned}
 \tag{13}$$

where squeeze number  $Sq < 0$  implies squeezing and  $Sq > 0$  corresponds to receding motion of the plates. Obtained

momentum equation (12) is subject to following non-dimensional boundary conditions after using equation (10) in equation (7)

$$\begin{aligned}
 U(0) &= 0, \\
 U''(0) &= 0, \\
 U(1) &= 1, \\
 U'(1) &= 0.
 \end{aligned}
 \tag{14}$$

**2.4. Model Verification.** To verify the fully fractional developed model, we put  $\alpha = 1$  in equation (12) and recover the following momentum equation derived in [45, 47].

$$Mg_t U^{(2)} - Mp_t U^{(2)} + Sq \left( UU^{(3)} - \eta U^{(3)} - 3U^{(2)} - U^{(2)}U' \right) + \left( \frac{1}{\beta} + 1 \right) U^{(4)}.
 \tag{15}$$

**2.5. Skin Friction.** The coefficient of skin friction is as follows:

$$C_f = \frac{\nu}{\nu_w^2} \left( 1 + \frac{1}{\beta} \right) \frac{\partial u}{\partial y} \Big|_{y=h(t)},
 \tag{16}$$

and after applying similarity transforms from equation (10) in above equation, we obtain dimensionless skin friction as follows:

$$\frac{L^2}{x^2(1 - \gamma t)} Re_x C_f = \left( 1 + \frac{1}{\beta} \right) U''(1),
 \tag{17}$$

where  $Re_x$  is the local Reynolds number  $[Re_x = 2L\nu_w^2/\nu x(1 - \gamma t)^{1/2}]$ .

### 3. Proposed Methodology for Fractional-Order Problem

To demonstrate the basic concept of modified homotopy perturbation algorithm [32], we firstly develop a homotopy as follows:

$$\mathfrak{L}\{\mathfrak{D}^\alpha\{\mathcal{P}[\mathcal{V}]\} + \mathfrak{D}^\alpha\{\mathcal{Q}[\mathcal{V}]\} - \mathfrak{F}(\mathbf{u})\} = 0, \quad r - 1 < \alpha \leq r,
 \tag{18}$$

where  $\mathcal{P}$  and  $\mathcal{Q}$  represent the linear and nonlinear parts of the function  $\mathcal{V}(\mathbf{u})$ , respectively.  $\mathfrak{D}^\alpha$  is the fractional differential operator and  $\mathfrak{F}(\mathbf{u})$  is some known function. In case of  $m^{th}$  order boundary value problems, dummy initial conditions are used to initialize the solution process.

In the next step, we construct a homotopy of given equation after applying definition of Laplace transform as follows:

$$H = (1 - q) \left( \mathfrak{L}\{\mathcal{V}(\mathbf{u})\} - \mathcal{V}_0 \right) + q \left( \mathfrak{L} \left\{ \mathcal{V}(\mathbf{u}) - \left( \frac{1}{s^\alpha} \right) \sum_{n=0}^{r-1} s^{\alpha-n-1} \mathcal{V}^{(n)}(0) + \left( \frac{1}{s^\alpha} \right) \mathfrak{L}\{\mathfrak{D}^\alpha\{\mathcal{Q}[\mathcal{V}]\} - \mathfrak{F}(\mathbf{u})\} \right\} \right),
 \tag{19}$$

where  $\mathcal{V}_0$  is the initial guess. Expansion of  $\mathcal{V}(\mathbf{u})$  in terms of power series gives the following equation:

$$\mathcal{V}(\mathbf{u}) = \sum_{i=0}^{\infty} q^i \mathcal{V}_i.
 \tag{20}$$

Substituting equation (20) in equation (19) and then comparing similar coefficients of  $q$  leads us to different order problems.

Problem at  $i$ -th order  $q^i$  is given as follows:

$$\mathfrak{L}\{\mathcal{V}_i(\mathbf{u})\} + \left(\frac{1}{s^\alpha}\right) \left( s^\alpha \mathfrak{L}\{\mathcal{Q}[\mathcal{V}_{i-1}]\} - \sum_{n=0}^{r-1} s^{\alpha-n-1} \mathcal{V}_{i-1}^{(n)}(0) \right) = 0. \quad (21)$$

Operating Laplace transform inverse gives the following equation:

$$\mathcal{V}_i(\mathbf{u}) + \mathfrak{L}^{-1} \left\{ \left(\frac{1}{s^\alpha}\right) \left( s^\alpha \mathfrak{L}\{\mathcal{Q}[\mathcal{V}_{i-1}]\} - \sum_{n=0}^{r-1} s^{\alpha-n-1} \mathcal{V}_{i-1}^{(n)}(0) \right) \right\} = 0. \quad (22)$$

Hence, the approximate solution of the fractional, nonlinear differential equation is as follows:

$$\begin{aligned} \tilde{\mathcal{V}} &= \lim_{q \rightarrow 1} \mathcal{V} \\ &= \sum_{i=0}^{\infty} \mathcal{V}_i(\mathbf{u}). \end{aligned} \quad (23)$$

In case BVPs, right side boundary conditions will be used to find optimal values of dummies constants of initial conditions. Residual errors of concerned fractional differential equation can be found by

$$\text{Res} = \mathfrak{D}^\alpha \{\mathcal{P}[\tilde{\mathcal{V}}]\} + \mathfrak{D}^\alpha \{\mathcal{Q}[\tilde{\mathcal{V}}]\} - \mathfrak{F}(\mathbf{u}). \quad (24)$$

## 4. Results and Discussion

In this section, initial numerical analysis at different values of fluid parameters is performed to check the efficiency and validity of the proposed approach in the case of unsteady squeezing of Casson fluid in fractional space. In next phase, the effects of different parameters on the normal and radial velocity are analyzed graphically. Our discussion of results is based on fractional and fluid parameters in the following subsections.

**4.1. Error Analysis and Numerical Validation.** Tables 1 and 2 show numerical validation and efficiency of the proposed methodology (modified homotopy perturbation algorithm) by comparing it with HPM and RK4 in the case of an unsteady squeezing flow of Casson fluid at  $\alpha = 1$ . In Table 1, residual error through modified HPM method varying between  $(0, \chi \times 10^{-14})$ . Similarly, Table 2 shows comparison of modified HPM results with HPM and RK4 at different values of non-Newtonian parameter  $\beta$ . In this case, modified HPM errors are varying in range  $(0, \chi \times 10^{-12})$ . Analysis of these tables shows that the current results obtained through the proposed methodology are better as compared to HPM and RK4. This analysis provides firm evidence for the validation and stability of the proposed methodology in the current study.

**4.2. Normal Velocity Profile.** Figures 1(a)–1(f) depict behavior of normal fluid velocity for increasing values of the fluid parameter  $\beta$ , the fractional parameter  $\alpha$ , the squeeze number  $Sq$ , an unsteady magnetic  $M_t$ , and porosity  $\kappa_t$  parameters. In Figure 1(a), with an increase in the fluid parameter  $\beta$  normal velocity shows different behavior about point  $\eta = 0.45$ . For  $\eta < 0.45$ , normal velocity increases with increasing fluid parameter, while decrease in fluid velocity in normal direction is observed for  $\eta > 0.45$ . Fractional parameter  $\alpha$  is varied between  $(0, 1)$  in Figure 1(b). Normal fluid velocity increases with increasing fractional parameter when  $0.3 < \eta < 0.8$  and it decreases otherwise. For squeezing motion of plates, i.e.,  $Sq < 0$  in Figure 1(c) velocity in normal direction decreases for  $\eta < 0.425$  and increases when  $\eta > 0.425$ . Contrasting behavior of velocity is observed in Figure 1(d) for receding motion between the two plates. The magnetic parameter  $M_t$  decreases normal fluid velocity for  $\eta < 0.5$  due to dominant Lorentz-like drag force on fluid flow. This drag force does not remain dominant after  $\eta = 0.5$  and hence velocity starts to increase in normal direction (see Figure 1(e)). Opposite behavior in case of higher porosity parameter  $\kappa_t$  is observed in Figure 1(f) about  $\eta = 0.5$ .

**4.3. Radial Velocity Profile.** Figures 2(a)–2(f) present simulations of radial velocity profile for fluid parameter  $\beta$ , fractional parameter  $\alpha$ , squeeze number  $Sq$ , unsteady magnetic  $M_t$  and porosity  $\kappa_t$  parameters. The velocity profile in radial direction shows increasing behavior in contrast to the normal velocity of the fluid. Radial velocity gradually increases with elevated non-Newtonian parameter  $\beta$  in Figure 2(a). The fractional parameter  $\alpha$  decreases fluid velocity in radial direction as seen in Figure 2(b). For squeeze number  $Sq < 0$ , i.e., when the plates are moving closer, velocity in radial direction decreases as observed in Figure 2(c). In contrast, radial velocity increases in the case of receding plates in Figure 2(d) as more space for fluid motion along the radius develops when plates are moving apart. An increase in the magnetic parameter  $M_t$  decreases radial velocity (see Figure 2(e)) due to a dominant drag force throughout the domain. In Figure 2(f) increase in fluid velocity is observed for higher values of the porosity parameter  $\kappa_t$ . The velocity

TABLE 1: Comparison of modified HPM results with RK4 and HPM for different Sq when  $\alpha = 1$ ,  $M_t = 0.5 = \kappa_t$ , and  $\beta = 0.05$ .

Parameters	$\eta$	Solution	Residual error		
			Modified HPM	RK4 [45]	HPM [45]
Sq = -0.2	0.1	0.149441	$8.67 \times 10^{-19}$	$6.59 \times 10^{-9}$	$9.93 \times 10^{-11}$
	0.3	0.436351	0	$2.71 \times 10^{-10}$	$5.16 \times 10^{-10}$
	0.5	0.687329	$2.78 \times 10^{-17}$	$2.41 \times 10^{-10}$	$5.33 \times 10^{-10}$
	0.7	0.878387	$2.08 \times 10^{-16}$	$5.29 \times 10^{-10}$	$1.53 \times 10^{-9}$
	0.9	0.985479	$2.87 \times 10^{-15}$	$1.08 \times 10^{-8}$	$1.17 \times 10^{-9}$
Sq = -0.4	0.1	0.1495	$8.67 \times 10^{-19}$	$3.68 \times 10^{-8}$	$5.03 \times 10^{-11}$
	0.3	0.436497	0	$2.33 \times 10^{-9}$	$1.52 \times 10^{-10}$
	0.5	0.687493	$2.30 \times 10^{-17}$	$5.65 \times 10^{-12}$	$5.45 \times 10^{-10}$
	0.7	0.878491	$2.65 \times 10^{-16}$	$1.86 \times 10^{-9}$	$2.09 \times 10^{-9}$
	0.9	0.985498	$1.76 \times 10^{-15}$	$2.54 \times 10^{-8}$	$1.81 \times 10^{-9}$
Sq = -0.6	0.1	0.149558	$6.94 \times 10^{-18}$	$8.03 \times 10^{-8}$	$1.24 \times 10^{-8}$
	0.3	0.436644	$1.39 \times 10^{-17}$	$5.07 \times 10^{-9}$	$3.79 \times 10^{-8}$
	0.5	0.687657	$1.53 \times 10^{-16}$	$3.17 \times 10^{-10}$	$7.21 \times 10^{-8}$
	0.7	0.878596	$4.75 \times 10^{-15}$	$4.49 \times 10^{-9}$	$1.42 \times 10^{-7}$
	0.9	0.985516	$5.06 \times 10^{-14}$	$6.40 \times 10^{-8}$	$3.01 \times 10^{-7}$

TABLE 2: Comparison of modified HPM results with RK4 and HPM for different values of  $\beta$  when  $\alpha = 1$ ,  $M_t = 0.5 = \kappa_t$ , and  $\beta = 0.05$ .

Parameters	$\eta$	Solution	Residual error		
			Modified HPM	RK4 [45]	HPM [45]
$\beta = 0.01$	0.1	0.149488	$2.17 \times 10^{-19}$	$8.33 \times 10^{-9}$	$8.92 \times 10^{-13}$
	0.3	0.436469	$8.67 \times 10^{-19}$	$2.87 \times 10^{-9}$	$4.63 \times 10^{-12}$
	0.5	0.687464	$2.60 \times 10^{-18}$	$2.45 \times 10^{-9}$	$4.79 \times 10^{-12}$
	0.7	0.878477	$3.47 \times 10^{-18}$	$1.89 \times 10^{-9}$	$1.37 \times 10^{-11}$
	0.9	0.985496	$3.47 \times 10^{-18}$	$2.78 \times 10^{-8}$	$1.05 \times 10^{-11}$
$\beta = 0.1$	0.1	0.149388	$6.94 \times 10^{-18}$	$1.83 \times 10^{-8}$	$6.91 \times 10^{-10}$
	0.3	0.436215	$6.94 \times 10^{-18}$	$1.08 \times 10^{-9}$	$3.59 \times 10^{-9}$
	0.5	0.687173	$2.78 \times 10^{-16}$	$2.80 \times 10^{-11}$	$3.71 \times 10^{-9}$
	0.7	0.878285	$9.80 \times 10^{-15}$	$8.24 \times 10^{-10}$	$1.06 \times 10^{-8}$
	0.9	0.985461	$1.38 \times 10^{-13}$	$1.16 \times 10^{-8}$	$8.20 \times 10^{-9}$
$\beta = 0.2$	0.1	0.149295	$3.47 \times 10^{-18}$	$3.03 \times 10^{-8}$	$4.25 \times 10^{-9}$
	0.3	0.435977	0	$2.07 \times 10^{-9}$	$2.21 \times 10^{-8}$
	0.5	0.686901	$9.84 \times 10^{-15}$	$1.63 \times 10^{-10}$	$2.28 \times 10^{-8}$
	0.7	0.878105	$3.71 \times 10^{-13}$	$1.87 \times 10^{-9}$	$6.57 \times 10^{-8}$
	0.9	0.985428	$5.22 \times 10^{-12}$	$2.73 \times 10^{-8}$	$5.05 \times 10^{-8}$

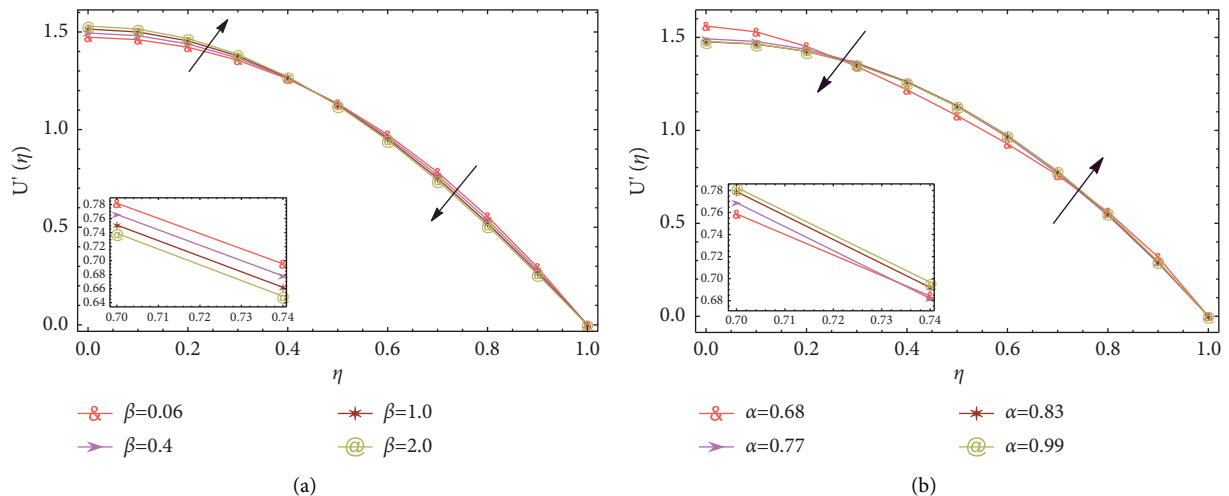


FIGURE 1: Continued.

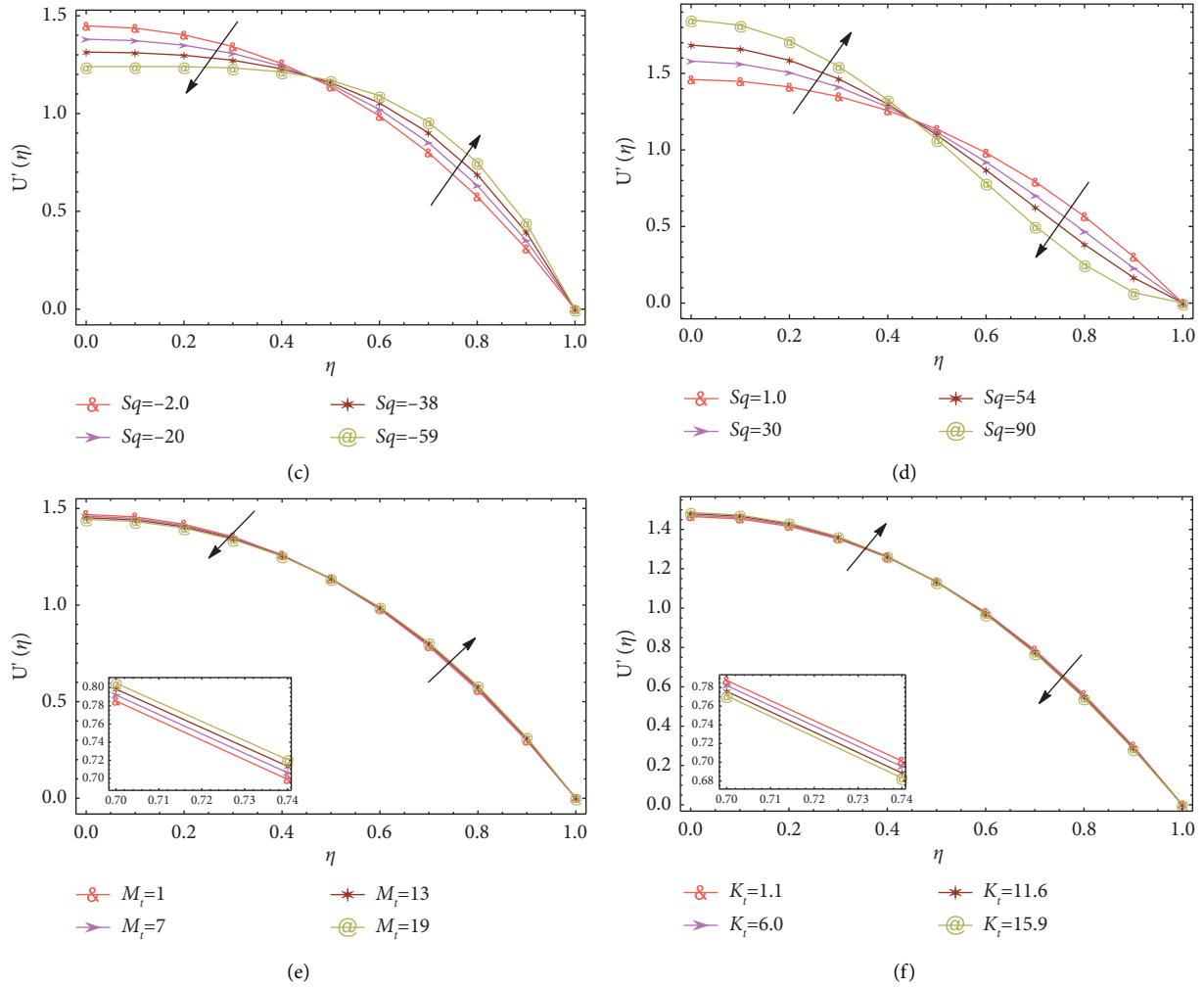


FIGURE 1: Effect of different parameters on normal velocity at  $\alpha = 0.85$ .

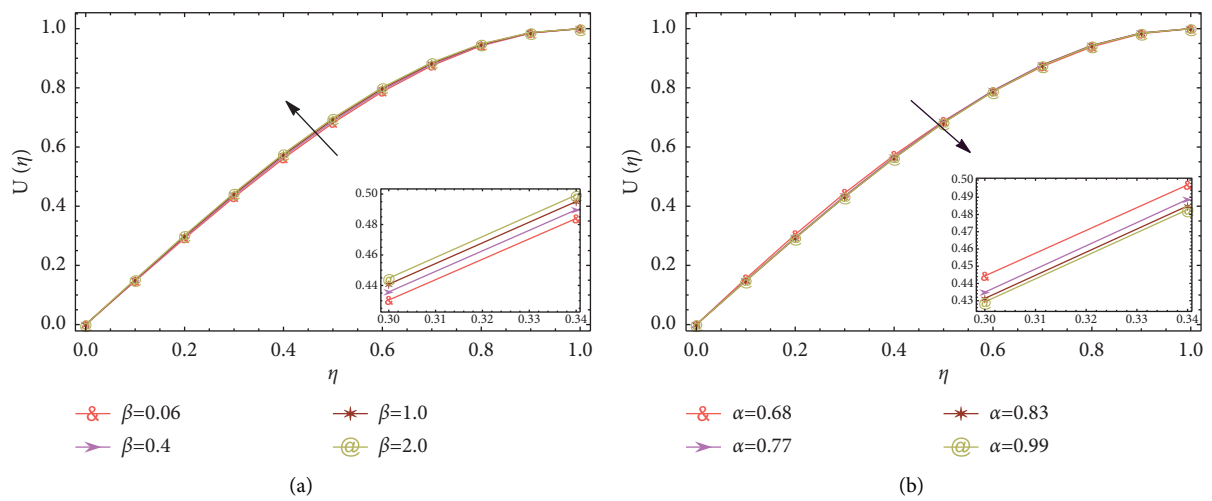


FIGURE 2: Continued.



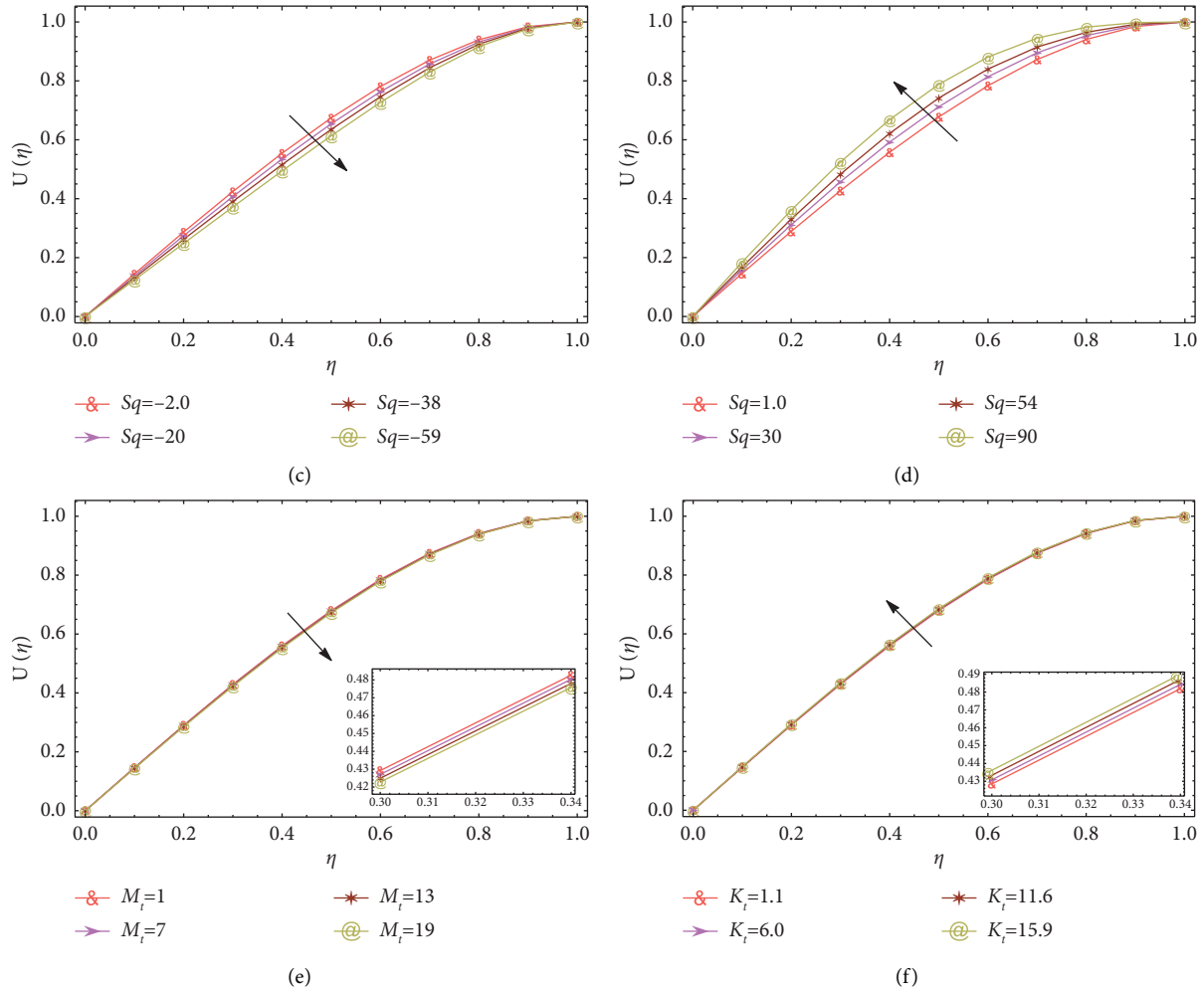


FIGURE 2: Effect of different parameters on radial velocity at  $\alpha = 0.85$ .

TABLE 3: Numerical values of skin friction for different values of  $\alpha, \beta, Sq, M_t$  and  $\kappa_t$ .

$\alpha$	$\beta$	Sq	$M_t$	$\kappa_t$	$(1 + 1/\beta)U''(1)$
0.65	2.0	0.70	0.80	1.50	-4.031
0.72					-4.413
0.85					-4.818
0.95					-4.852
0.80	0.90				-6.618
	1.30				-5.539
	2.40				-4.426
	3.00				-4.162
	1.00	0.34			-6.286
		0.98			-6.253
		1.56			-6.223
		2.50			-6.175
		0.70	0.50		-6.263
			0.90		-6.269
			1.50		-6.279
			2.00		-6.292
			1.10	0.20	-6.293
				0.87	-6.282
				1.60	-6.271
				2.80	-6.252

boundary layer is enhanced with higher values of  $\kappa_t$  due to which resistance among fluid layers decreases causing an increase in fluid velocity along radial direction.

4.4. *Skin Friction.* Skin friction at the wall  $y = h(t)$  is simulated numerically in Table 3 against the fractional parameter  $\alpha$ , fluid parameter  $\beta$ , squeeze number Sq, magnetic parameter  $M_t$ , and porosity parameter  $\kappa_t$ . It is observed that increase in  $\alpha$  and  $M_t$  increases the skin friction at the boundary. Moreover, an increase in  $\beta$ , Sq, and  $\kappa_t$  decreases the skin friction of fractional Casson fluid.

### 5. Conclusions

The objective of the current manuscript is fractional modeling and simulation of the unsteady squeezing flow of Casson fluid. The incompressible Casson fluid is considered to have MHD and Darcian effects in a fully fractional environment. The obtained model is validated by recovering the ODE of integer-order at  $\alpha = 1$ . In current modeling, the obtained equations are fractionally transformed, and solved through modified homotopy perturbation algorithm. An error analysis is performed for checking the convergence

and validity of the applied methodology. It is noted that the solutions are improved using modified HPM as compared to existing results in the literature. The key findings of this study are as follows:

- (i) Radial velocity increases throughout the domain in contrast to normal fluid velocity.
- (ii) Decrease in radial velocity is observed against increasing  $M_t$ ,  $Sq < 0$  and  $\alpha$  whereas radial velocity increases in case of higher  $\kappa_t$ ,  $\beta$  and  $Sq > 0$ .
- (iii) Velocity in normal direction shows similar behavior as radial velocity for  $\eta < \chi$  and inverse behavior is observed when  $\eta > \chi$ .
- (iv) Furthermore, the squeeze number and porosity parameter present opposite behavior in fractional enthronelement when compared with the existing integer-order model given in [45].

This study provides the basis for fractional modeling of the unsteady squeezed flow of Casson fluid in particular and non-Newtonian fluid in general. The steps presented in current modeling can be extended to different non-Newtonian fluid models like Maxwell, Carreau, and Sutterby fluids under various boundary conditions.

## Nomenclature

$(x, y)$ :	Spatial coordinates (m)
$t$ :	Temporal coordinate (s)
$(u, v)$ :	Velocities in $x$ and $y$ directions ( $\text{ms}^{-1}$ )
$\tau$ :	Extra stress tensor ( $\text{kgm}^{-1}\text{s}^2$ )
$e_{i,j}$ :	Rate of deformation
$L$ :	Initial gap between plates (m)
$\gamma$ :	Constant quantity ( $\text{s}^{-1}$ )
$\mu$ :	Dynamic viscosity ( $\text{kgm}^{-1}\text{s}^{-1}$ )
$P_y$ :	Yield stress (Pa)
$\rho$ :	Density ( $\text{kgm}^{-3}$ )
$B$ :	Magnetic field strength ( $\text{Am}^{-1}$ )
$\beta$ :	Casson fluid parameter
$\sigma$ :	Electric conductivity ( $\text{Sm}^{-1}$ )
$\nu$ :	Kinematic viscosity ( $\text{m}^2\text{s}^{-1}$ )
$k$ :	Porosity rate ( $\text{m}^2$ ).

## Data Availability

All the data are available within manuscript.

## Conflicts of Interest

The authors declare that they have no conflicts of interest.

## References

- [1] Y. M. Chu, M. D. Ikram, M. A. Imran, and A. Akgül, "MHD flow of a Newtonian fluid in symmetric channel with ABC fractional model containing hybrid nanoparticles," *Combinatorial Chemistry & High Throughput Screening*, vol. 25, no. 7, pp. 1087–1102, 2022.
- [2] Y. Kang, S. Mao, and Y. Zhang, "Fractional time-varying grey traffic flow model based on viscoelastic fluid and its application," *Transportation Research Part B: Methodological*, vol. 157, pp. 149–174, mar 2022.
- [3] M. Yavuz, N. Sene, and M. Yıldız, "Analysis of the influences of parameters in the fractional second-grade fluid dynamics," *Mathematics*, vol. 10, no. 7, p. 1125, 2022.
- [4] K. A. Abro, "Role of fractal fractional derivative on ferro-magnetic fluid via fractal laplace transform: a first problem via fractal fractional differential operator," *European Journal of Mechanics - B: Fluids*, vol. 85, pp. 76–81, 2021.
- [5] L. Chen, C. Tian, P. Cui, K. Zhang, and Y. An, "Bursty data service latency analysis under fractional calculus fluid model of multi-hop wireless networks," *Wireless Networks*, vol. 27, no. 7, pp. 4403–4409, jun 2021.
- [6] K. A. Abro and A. Atangana, "Dual fractional modeling of rate type fluid through non-local differentiation," *Numerical Methods for Partial Differential Equations*, vol. 38, Article ID 22633, 2020.
- [7] R. Reyaz, Y. J. Lim, Q. Ahmad, M. Saqib, and S. Shafie, "Caputo fractional MHD casson fluid flow over an oscillating plate with thermal radiation," *Journal of Advanced Research in Fluid Mechanics and Thermal Sciences*, vol. 85, no. 2, pp. 145–158, 2021.
- [8] M. Arif, P. Kumam, W. Kumam, I. Khan, and M. Ramzan, "A fractional model of casson fluid with ramped wall temperature: engineering applications of engine oil," *Computational and Mathematical Methods*, vol. 3, no. 6, 2021.
- [9] N. Sarwar, M. I. Asjad, T. Sitthiwiratham, N. Patanarapeelert, and T. Muhammad, "A prabhakar fractional approach for the convection flow of casson fluid across an oscillating surface based on the generalized fourier law," *Symmetry*, vol. 13, no. 11, p. 2039, 2021.
- [10] A. Ur Rehman, M. B. Riaz, and A. Atangana, "Time fractional analysis of casson fluid with rabotnov exponential memory based on the generalized fourier and ficks law," *Scientific African*, vol. 17, Article ID e01385, 2022.
- [11] S. Murtaza, P. Kumam, Z. Ahmad, K. Sitthithakerngkiet, and I. E. Ali, "Finite difference simulation of fractal-fractional model of electro-osmotic flow of casson fluid in a micro channel," *IEEE Access*, vol. 10, Article ID 26681, 2022.
- [12] B. J. Gireesha, B. Mahanthesh, R. S. R. Gorla, and K. L. Krupalakshmi, "Mixed convection two-phase flow of Maxwell fluid under the influence of non-linear thermal radiation, non-uniform heat source/sink and fluid-particle suspension," *Ain Shams Engineering Journal*, vol. 9, no. 4, pp. 735–746, 2018.
- [13] B. Mahanthesh, B. J. Gireesha, G. T. Thammanna, S. A. Shehzad, F. M. Abbasi, and R. S. R. Gorla, "Nonlinear convection in nano Maxwell fluid with nonlinear thermal radiation: a three-dimensional study," *Alexandria Engineering Journal*, vol. 57, no. 3, pp. 1927–1935, 2018.
- [14] K. L. Krupalakshmi, B. J. Gireesha, B. Mahanthesh, and R. S. R. Gorla, "Influence of nonlinear thermal radiation and magnetic field on upper-convected Maxwell fluid flow due to a convectively heated stretching sheet in the presence of dust particles," *Communications in Numerical Analysis*, vol. 2016, no. 1, pp. 57–73, 2016.
- [15] S. Das, S. Sarkar, and R. N. Jana, "Feature of entropy generation in cu-al2o3/ethylene glycol hybrid nanofluid flow through a rotating channel," *BioNanoScience*, vol. 10, no. 4, pp. 950–967, 2020.
- [16] B. Mahanthesh, "Flow and heat transport of nanomaterial with quadratic radiative heat flux and aggregation kinematics of nanoparticles," *International Communications in Heat and Mass Transfer*, vol. 127, Article ID 105521, 2021.

- [17] B. B. Divya, G. Manjunatha, C. Rajashekhar, H. Vaidya, and K. V. Prasad, "Analysis of temperature dependent properties of a peristaltic MHD flow in a non-uniform channel: a casson fluid model," *Ain Shams Engineering Journal*, vol. 12, no. 2, pp. 2181–2191, 2021.
- [18] M. W. S. Khan and N. Ali, "Theoretical analysis of thermal entrance problem for blood flow: an extension of classical graetz problem for casson fluid model using generalized orthogonality relations," *International Communications in Heat and Mass Transfer*, vol. 109, Article ID 104314, 2019.
- [19] S. M. M. El-Kabeir, E. R. El-Zahar, and A. M. Rashad, "Effect of chemical reaction on heat and mass transfer by mixed convection flow of casson fluid about a sphere with partial slip," *Journal of Computational and Theoretical Nanoscience*, vol. 13, no. 8, pp. 5218–5226, 2016.
- [20] M. Aneja, A. Chandra, and S. Sharma, "Natural convection in a partially heated porous cavity to casson fluid," *International Communications in Heat and Mass Transfer*, vol. 114, Article ID 104555, 2020.
- [21] M. Hamid, M. Usman, Z. H. Khan, R. U. Haq, and W. Wang, "Heat transfer and flow analysis of casson fluid enclosed in a partially heated trapezoidal cavity," *International Communications in Heat and Mass Transfer*, vol. 108, Article ID 104284, 2019.
- [22] M. Rashidi, Z. Yang, M. Bhatti, and M. Abbas, "Heat and mass transfer analysis on MHD blood flow of casson fluid model due to peristaltic wave," *Thermal Science*, vol. 22, no. 6, pp. 2439–2448, 2018.
- [23] S. Das, S. Sarkar, and R. N. Jana, "Entropy generation analysis of mhd slip flow of non-Newtonian cu-casson nanofluid in a porous microchannel filled with saturated porous medium considering thermal radiation," *Journal of Nanofluids*, vol. 7, no. 6, pp. 1217–1232, 2018.
- [24] S. Das, S. Sarkar, and R. N. Jana, "Entropy generation minimization of magnetohydrodynamic slip flow of casson  $H_2O + Cu$  nanofluid in a porous microchannel," *Journal of Nanofluids*, vol. 8, no. 1, pp. 205–221, 2019.
- [25] S. K. Vs and N. P. Pai, "Suction and injection effect on flow between two plates with reference to casson fluid model," *Multidiscipline Modeling in Materials and Structures*, vol. 15, no. 3, pp. 559–574, 2019.
- [26] A. S. Hamarshah, F. A. Alwawi, H. T. Alkassabeh, A. M. Rashad, and R. Idris, "Heat transfer improvement in MHD natural convection flow of graphite oxide/carbon nanotubes-methanol based casson nanofluids past a horizontal circular cylinder," *Processes*, vol. 8, no. 11, p. 1444, 2020.
- [27] F. A. Alwawi, H. T. Alkassabeh, A. M. Rashad, and R. Idris, "A numerical approach for the heat transfer flow of carboxymethyl cellulose-water based casson nanofluid from a solid sphere generated by mixed convection under the influence of lorentz force," *Mathematics*, vol. 8, no. 7, p. 1094, 2020.
- [28] F. A. Alwawi, H. T. Alkassabeh, A. M. Rashad, and R. Idris, "MHD natural convection of sodium alginate casson nanofluid over a solid sphere," *Results in Physics*, vol. 16, Article ID 102818, 2020.
- [29] E. R. El-Zahar, A. E. N. Mahdy, A. M. Rashad, W. Saad, and L. F. Seddek, "Unsteady MHD mixed convection flow of non-Newtonian casson hybrid nanofluid in the stagnation zone of sphere spinning impulsively," *Fluid*, vol. 6, no. 6, p. 197, 2021.
- [30] S. Das, A. S. Banu, and R. N. Jana, "Delineating impacts of non-uniform wall temperature and concentration on time-dependent radiation-convection of casson fluid under magnetic field and chemical reaction," *World Journal of Engineering*, vol. 18, no. 5, pp. 780–795, 2021.
- [31] V. F. Morales-Delgado, J. F. Gómez-Aguilar, S. Kumar, and M. A. Taneco-Hernández, "Analytical solutions of the keller-segel chemotaxis model involving fractional operators without singular kernel," *The European Physical Journal Plus*, vol. 133, no. 5, p. 200, 2018.
- [32] M. Qayyum, E. Ahmad, M. B. Riaz, J. Awrejcewicz, and S. T. Saeed, "New soliton solutions of time-fractional korteweg-de vries systems," *Universe*, vol. 8, no. 9, p. 444, 2022.
- [33] K. Nonlaopon, M. Naeem, A. M. Zidan, R. Shah, A. Alsanad, and A. Gumaei, "Numerical investigation of the time-fractional whitham-broer-kaup equation involving without singular kernel operators," *Complexity*, vol. 2021, Article ID 7979365, 21 pages, 2021.
- [34] T. A. Sulaiman, M. Yavuz, H. Bulut, and H. M. Baskonus, "Investigation of the fractional coupled viscous burgers' equation involving mittag-leffler kernel," *Physica A: Statistical Mechanics and Its Applications*, vol. 527, Article ID 121126, 2019.
- [35] S. Ahmad, A. Ullah, K. Shah, and A. Akgül, "Computational analysis of the third order dispersive fractional pde under exponential-decay and mittag-leffler type kernels," *Numerical Methods for Partial Differential Equations*, pp. 1–16, 2020.
- [36] R. Shokhanda, P. Goswami, J.-H. He, and A. Althobaiti, "An approximate solution of the time-fractional two-mode coupled burgers equation," *Fractal and Fractional*, vol. 5, no. 4, p. 196, nov 2021.
- [37] M. Yavuz and N. Ozdemir, "Numerical inverse laplace homotopy technique for fractional heat equations," *Thermal Science*, vol. 22, no. 1, pp. 185–194, 2018.
- [38] P. Pandey, S. Kumar, and F. Gómez, "Approximate analytical solution of two-dimensional space-time fractional diffusion equation," *Mathematical Methods in the Applied Sciences*, vol. 43, no. 12, pp. 7194–7207, 2020.
- [39] J. Fang, M. Nadeem, and H. A. Wahash, "A semianalytical approach for the solution of nonlinear modified camassa-holm equation with fractional order," *Journal of Mathematics*, vol. 2022, Article ID 5665766, 8 pages, 2022.
- [40] P. Pandey, S. Kumar, J. F. Gómez-Aguilar, and D. Baleanu, "An efficient technique for solving the space-time fractional reaction-diffusion equation in porous media," *Chinese Journal of Physics*, vol. 68, pp. 483–492, 2020.
- [41] H. Zhang, M. Nadeem, A. Rauf, and Z. Guo Hui, "A novel approach for the analytical solution of nonlinear time-fractional differential equations," *International Journal of Numerical Methods for Heat & Fluid Flow*, vol. 31, no. 4, pp. 1069–1084, 2020.
- [42] B. Jalili, P. Jalili, A. Shateri, and D. D. Ganji, "Rigid plate submerged in a Newtonian fluid and fractional differential equation problems via caputo fractional derivative," *Partial Differential Equations in Applied Mathematics*, vol. 6, Article ID 100452, 2022.
- [43] S. Jiang, J. Zhang, Q. Zhang, and Z. Zhang, "Fast evaluation of the caputo fractional derivative and its applications to fractional diffusion equations," *Communications in Computational Physics*, vol. 21, no. 3, pp. 650–678, feb 2017.
- [44] N. H. Tuan, H. Mohammadi, and S. Rezapour, "A mathematical model for COVID-19 transmission by using the caputo fractional derivative," *Chaos, Solitons & Fractals*, vol. 140, Article ID 110107, 2020.
- [45] H. Khan, M. Qayyum, O. Khan, and M. Ali, "Unsteady squeezing flow of casson fluid with magnetohydrodynamic

- effect and passing through porous medium,” *Mathematical Problems in Engineering*, vol. 2016, Article ID 4293721, 14 pages, 2016.
- [46] A. Saeed, M. Bilal, T. Gul, P. Kumam, A. Khan, and M. Sohail, “Fractional order stagnation point flow of the hybrid nanofluid towards a stretching sheet,” *Scientific Reports*, vol. 11, no. 1, Article ID 20429, 2021.
- [47] N. A. Mat Noor, S. Shafie, and M. A. Admon, “MHD squeezing flow of casson nanofluid with chemical reaction, thermal radiation and heat generation/absorption,” *Journal of Advanced Research in Fluid Mechanics and Thermal Sciences*, vol. 68, no. 2, pp. 94–111, 2020.